

Waves and Instabilities in Rotating and Stratified Flows

Patrice Le Gal

Abstract This review intended primarily for Master degree students, presents the different types of classical waves that can occur in astro and geophysical flows. Inertial waves, caused by the rotation of the fluid, will first be introduced as well as their 2D version called Rossby waves. Then it will be shown how a density stratification of the fluid can make internal gravity waves appear. In each case and in the case where both rotation and stratification are present, the dispersion relations of the waves are derived. A differential rotation will then be added on the flow. The classical Rayleigh criterium for the centrifugal instability is recovered in the case of an homogeneous fluid but it will be shown that a new instability, called the strato-rotational instability (SRI), can occur when the fluid is stratified. Some experiments will be described. Finally, we will show how the application of a magnetic field can create Alfven waves in a rotating electrically conducting fluid and in which conditions the magneto-rotational instability (MRI) can grow.

1 Inertial Waves

First, let us consider an inviscid fluid of density ρ rotating around an axis \overrightarrow{Oz} at a rate $\overrightarrow{\Omega}$. The linearized Euler equation for the perturbed velocity \overrightarrow{u} and pressure field p describing the flow reads in the rotating frame of reference:

P. Le Gal (✉)

Institut de Recherche sur les Phénomènes Hors Equilibre, UMR 6594,
CNRS—Aix-Marseille Université, 49 rue F. Joliot Curie,
13384 Marseille, Cédex 13, France
e-mail: legal@irphe.univ-mrs.fr

$$\frac{\partial \vec{u}}{\partial t} + 2\vec{\Omega} \wedge \vec{u} = \frac{-\vec{\nabla} p}{\rho} \quad (1)$$

As can be seen, the Coriolis force appears here as a restoring force, forcing the displaced fluid particles to move on circles. The Coriolis force is the generating force of waves called “inertial waves” or “Kelvin waves” (Kelvin 1880). Searching for a local solution (in opposition to a global one where the geometry and boundary conditions are taken into account) of Eq. 1 under the form of a plane wave with a frequency ω and a wave vector $\vec{k} = (\alpha, \beta, \gamma)$: $(u, v, w, p/\rho) = (\hat{u}, \hat{v}, \hat{w}, \hat{p})e^{i(\alpha x + \beta y + \gamma z - \omega t)}$, we find easily the following algebraic system of equations:

$$\begin{cases} -i\omega\hat{u} & -2\Omega\hat{v} & = -i\alpha\hat{p} \\ -i\omega\hat{v} + 2\Omega\hat{u} & & = -i\beta\hat{p} \\ -i\omega\hat{w} & & = -i\gamma\hat{p} \end{cases} \quad (2)$$

This set of equations can be completed by the divergence free flow hypothesis that reads in the Fourier space as the following:

$$i\alpha\hat{u} + i\beta\hat{v} + i\gamma\hat{w} = 0 \quad (3)$$

Eliminating the pressure and velocity fields from these four equations leads to the well known dispersion relation of the Kelvin or inertial waves:

$$\omega^2 = \frac{4\gamma^2\Omega^2}{\alpha^2 + \beta^2 + \gamma^2} \quad (4)$$

This dispersion relation is special in the sense that the angle θ of propagation of a wave beam versus the rotation axis is simply given by the frequency of the waves:

$$\omega^2 = 4\Omega^2 \cos^2(\theta) \quad (5)$$

Another characteristic of inertial waves is that their phase velocity is perpendicular to their group velocity. In order to illustrate the shape of the dispersion relation curve, we can fix the values of wavenumbers α and β and plot ω as functions of the axial wavenumber γ . Figure 1 shows that the frequencies are confined between $\pm 2\Omega$.

A classical way to produce these waves in the laboratory is to vibrate an object in a rotating tank at a given frequency. As explained before, the angle of propagation of the waves is determined by their frequency and thus the periodic fluid motions take place along cones emerging from the oscillating generator. Figure 2b is taken from an experiment by Messio et al. (2008) and Courtesy of University of Paris where the velocity field is measured by PIV in a plane perpendicular to the axis of rotation (which was here also the axis of vibration of a small cylinder).

Of course, as in a real fluid these waves are damped by viscosity, they need to be excited as we just saw in the previous experiment. However, the shape of the dispersion relations of inertial waves permits also parametric resonances to appear

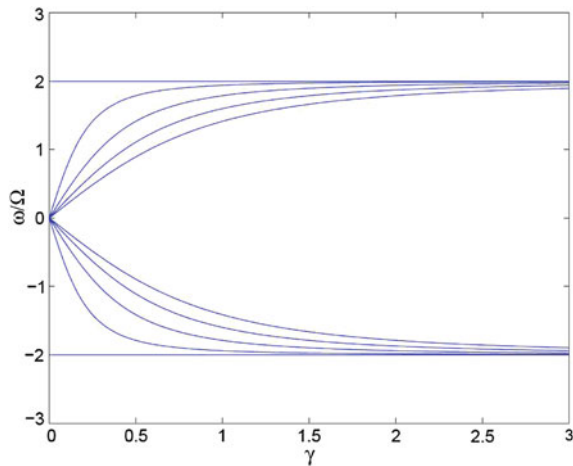


Fig. 1 Some dispersion relation curves of the Kelvin inertial waves as functions of axial wavenumber γ for various α and β

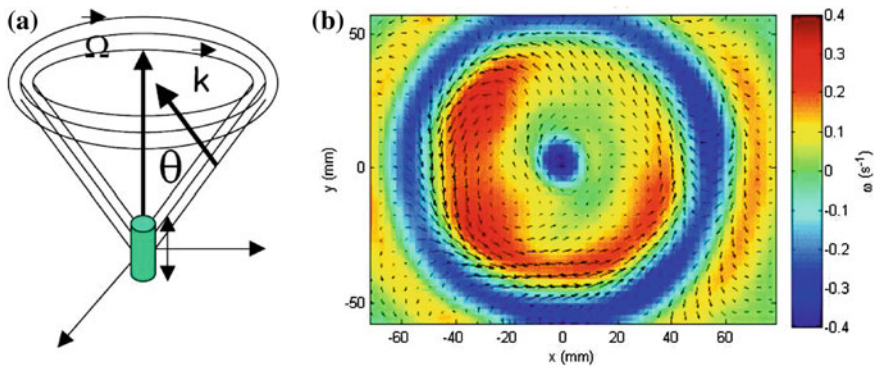


Fig. 2 **a** Schematic representation of the Kelvin wave cone generated by an oscillating cylinder in a rotating fluid. **b** Embarqued PIV measurements of the velocity field of a Kelvin wave conical beam generated by a vibrating cylinder, from Courtesy of University of Paris

under certain forcing conditions like those produced by precession, libration or tidal deformations of the rotating container. These resonances can indeed trigger the growth and interaction of inertial waves above a certain threshold. For instance, when a cylindrical rotating container is elliptically deformed in its cross section, two Kelvin waves can resonate with the elliptical deformation of the streamlines. An instability, called the elliptical instability can appear when these resonant conditions are met (Eloy et al. 2003). This instability is known to affect the vortices behind airplanes but can also play a role in astro and geophysics. Indeed, a planetary molten iron core flow could very well be destabilized by the

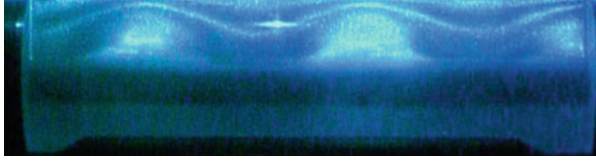


Fig. 3 Visualization of the elliptical instability of a tidally distorted deformable rotating cylindrical shell. In this illustration, the unstable mode is oscillating at a pulsation equal to Ω and corresponds to a resonance between two Kelvin waves with azimuthal wavenumbers 0 and 2

tidal distortions induced by a closed orbiting object (Lacaze et al. 2005; Cébron et al. 2010). Figure 3 presents a visualization of the elliptical instability in a rotating cylindrical shell where a Laser plane is sent in the meridional plane and illuminates Kalliroscope particles.

2 A Particular Case of Inertial Waves: The Rossby Waves

Laboratory observations of inertial waves are not easy and we saw in Sect. 1 that it was only relatively recently that these waves have been precisely measured when excited in a rotating tank. However, a particular case of these waves are known from a long time in meteorology. These waves called Rossby waves (Rossby 1939) can be described using first a bi-dimensional approximation of Eq. 1 ($\frac{\partial}{\partial z} = 0$ and $w = 0$), second when taking into account a linear variation of the Coriolis parameter 2Ω with the latitude (the β plane approximation). The flow is then described by the following equations:

$$\begin{cases} \frac{\partial u}{\partial t} - 2\Omega(y)v = -\frac{1}{\rho}\frac{\partial p}{\partial x} \\ \frac{\partial v}{\partial t} + 2\Omega(y)u = -\frac{1}{\rho}\frac{\partial p}{\partial y} \end{cases} \quad (6)$$

with $\frac{\partial \Omega(y)}{\partial y} = \beta_c$. The variation in time of the axial vorticity Ω_z of the two-dimensional motion can then easily be expressed as:

$$\frac{\partial \Omega_z}{\partial t} + 2\beta_c v = 0 \quad (7)$$

As in Sect. 1, this equation is completed by the incompressibility condition and taking their Fourier transforms leads to the following dispersion of the Rossby waves:

$$\omega = \frac{-2\beta_c \alpha}{\alpha^2 + \beta^2} \quad (8)$$

Fig. 4 Some dispersion relation curves of the Rossby waves as functions of the azimuthal wavenumber α for various β

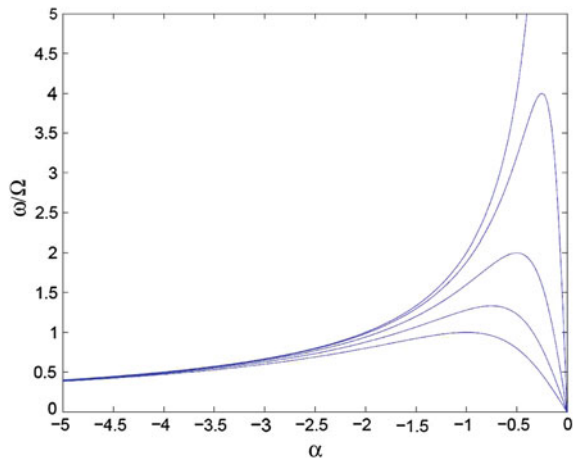
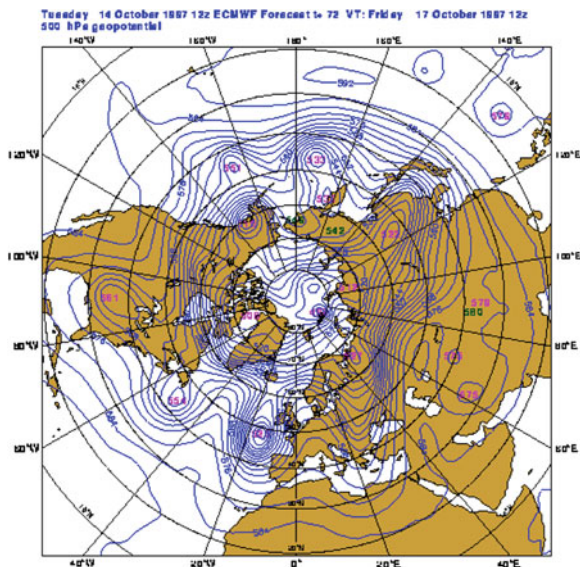


Fig. 5 Illustration of the propagation of a Rossby wave in the atmosphere, from Courtesy of University of Oregon (1999)



As can be seen from this dispersion relation, the phase velocity of the Rossby waves is $\frac{\omega}{\alpha} < 0$ and this is the reason why Rossby waves propagate westward in the Northern atmosphere. As in Sect. 1 we can fix the values of the wavenumbers β and plot in Fig. 4 the frequency ω as functions of the azimuthal wavenumber α . Classical meteorological images used for weather forecast give good illustrations of the propagation of the Rossby waves in the atmosphere. The succession of cyclonic and anticyclonic structures in the pressure field circumtravel around the North Pole as illustrated in Fig. 5.

Fig. 6 Illustration of the propagation of a Rossby wave in a rotating tank with a tilted bottom, from Courtesy of University of Washington

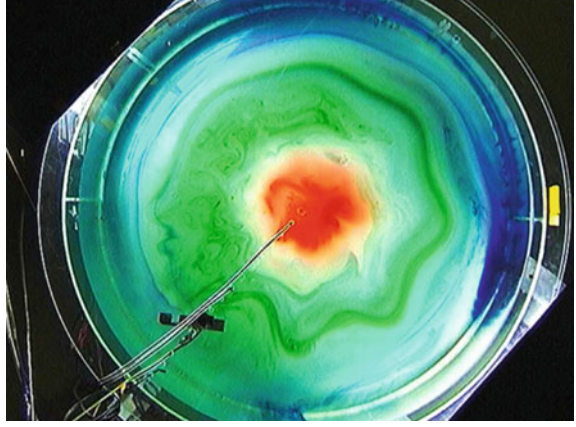
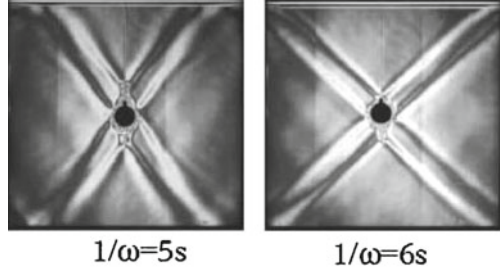


Fig. 7 Shadowgraph visualizations of the St Andrew cross formed by the four internal wave beams generated by a vertically vibrated small cylinder in a stratified layer of salt water, from Courtesy of Sakai, Iizawa, Aramaki (1997)



These waves can be reproduced in laboratory experiments using rotating tanks at constant rate Ω that possess tilted bottoms at an angle $\hat{\theta}$. The three-dimensional inviscid equation that describes the fluid motions in the rotating frame of reference is Eq. 1. Taking the curl and then using the divergenceless property of the flow, leads to the equation of the axial vorticity Ω_z :

$$\frac{\partial \Omega_z}{\partial t} = -2\Omega \frac{\partial w}{\partial z} \quad (9)$$

If we search solutions for u and v that are invariant along the z axis (the geostrophic hypothesis), the z derivative of the former equation gives: $\frac{\partial^2 w}{\partial z^2} = 0$. The vertical component of the velocity is therefore a linear function of the axial coordinate z : $w = az + b$. Applying the boundary conditions ($w = 0$) on the top surface supposed at $z = 0$ and at the bottom at $z = -h$ ($v_{\perp} = w(t, x, -h) \cos \hat{\theta} + v(t, x, -h) \sin \hat{\theta} = 0$) permits to link the axial velocity w and the velocity v perpendicular to the axis of rotation in a neighborhood of x where h is supposed constant:

$$\frac{\partial \Omega_z}{\partial t} = 2 \frac{\Omega \tan \hat{\theta}}{h} v(t, x, h) \quad (10)$$

Equation 10 is analogous to Eq. 7 where the β effect is given by $\beta_c = 2 \frac{tg\hat{\theta}}{h}$. This analogy leads to the dispersion relation of Rossby waves in rotating tanks with tilted bottoms:

$$\omega = -2 \frac{\Omega tg\hat{\theta}}{h\alpha} \quad (11)$$

Figure 6 illustrates this analogy where an oscillating cylinder generates wave trains visualized by dye in a rotating tank with a tilted bottom.

3 Gravity Waves

Often, planetary atmospheres or oceans are stably stratified in the vertical direction \overrightarrow{Oz} leading to the existence of a new set of waves called gravity or internal waves. Starting with no rotation, the linearized equations of motion for a stratified flow are:

$$\begin{cases} \frac{\partial u}{\partial t} = -\frac{1}{\rho} \frac{\partial p}{\partial x} \\ \frac{\partial v}{\partial t} = -\frac{1}{\rho} \frac{\partial p}{\partial y} \\ \frac{\partial w}{\partial t} = -\frac{1}{\rho} \frac{\partial p}{\partial z} + b \\ \frac{\partial b}{\partial t} = -N^2 w \end{cases} \quad (12)$$

where the buoyancy force is approximated by the first term of its Taylor expansion: $\overrightarrow{b} = \frac{1}{\rho} \frac{\partial \rho}{\partial z} \overrightarrow{g} z$. Traditionally, the vertical gradient of density is written in term of a Brunt-Väisälä frequency N which is defined by: $N^2 = -\frac{1}{\rho} \frac{\partial \rho}{\partial z} g$. As before, taking the Fourier transform of the linearized Euler equation leads to the algebraic set of equations:

$$\begin{cases} -i\omega \hat{u} = -i\alpha \hat{p} \\ -i\omega \hat{v} = -i\beta \hat{p} \\ -i\omega \hat{w} = -i\gamma \hat{p} + \hat{b} \\ -i\omega \hat{b} = -N^2 \hat{w} \end{cases} \quad (13)$$

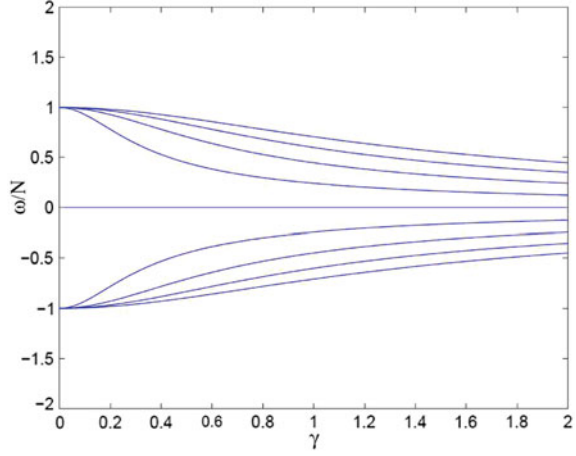
which leads to the dispersion relation of internal gravity waves:

$$\omega^2 = N^2 \frac{\alpha^2 + \beta^2}{\alpha^2 + \beta^2 + \gamma^2} \quad (14)$$

Or, if we note θ the angle of the wave vector versus the vertical axis of stratification:

$$\omega^2 = N^2 \sin^2(\theta) \quad (15)$$

Fig. 8 Some dispersion relation curves of the internal waves as functions of axial wavenumber γ for various α and β values



Comparing both dispersion relations (5) and (15), the parallel between inertial and internal waves is striking. This confers to both systems of waves similar characteristics: for instance, their frequency determines the angle of propagation of the beams and their phase and group velocities are perpendicular one to the other respectively. Figure 7 shows two shadowgraph images of the St-Andrew cross generated by the oscillation of a small cylinder in a salt stratified layer of water (Courtesy of Sakai, Iizawa, Aramaki 1997). As explained before, it can be observed that changing the excitation frequency changes the angle of the wave beams.

The dispersion relation given by Eq. 14 can be illustrated by plotting ω as functions of γ for different values of α and β . Because of the form of this dispersion relation, Fig. 8 shows that the frequencies of internal waves are confined between $\pm N$.

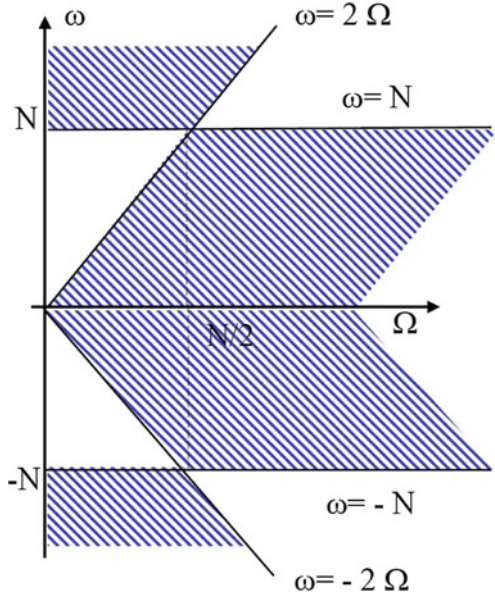
4 Gravito-Inertial Waves

Rotation and stratification versus \overrightarrow{Oz} can be taken into account together to study gravito-inertial waves. The linearization of the Euler equations written in the rotating frame of reference gives the following system of equations:

$$\left\{ \begin{array}{lcl} \frac{\partial u}{\partial t} - 2\Omega v & = & -\frac{1}{\rho} \frac{\partial p}{\partial x} \\ \frac{\partial v}{\partial t} + 2\Omega u & = & -\frac{1}{\rho} \frac{\partial p}{\partial y} \\ \frac{\partial w}{\partial t} & = & -\frac{1}{\rho} \frac{\partial p}{\partial z} + b \\ \frac{\partial b}{\partial t} & = & -N^2 w \end{array} \right. \quad (16)$$

with the same notation as before. The Fourier transform of this system of differential equations leads naturally to the dispersion relation of the gravito-inertial waves:

Fig. 9 Conditions of existence of gravito-inertial waves in the (ω, N) plane. Two distinct domains of existence (*empty areas*) are defined by the lines $\omega = \pm N$ and $\omega = \pm 2\Omega$



$$\omega^2 = \frac{4\gamma^2\Omega^2 + N^2(\alpha^2 + \beta^2)}{\alpha^2 + \beta^2 + \gamma^2} \quad (17)$$

which writes also as a function of the angle θ of the wave vector versus the vertical axis of rotation:

$$\omega^2 = 4\Omega^2 \cos^2(\theta) + N^2 \sin^2(\theta) \quad (18)$$

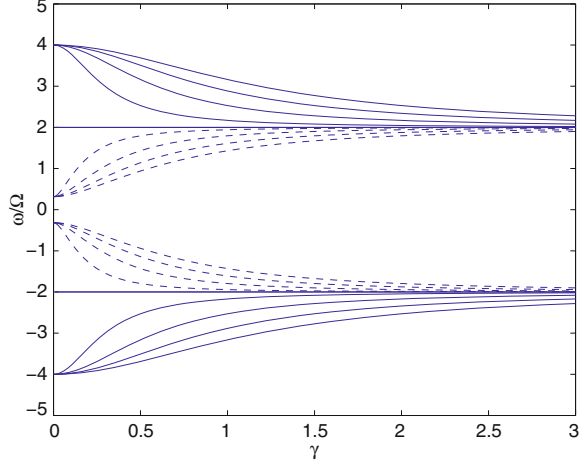
Note that this dispersion relation was only quite recently studied in Peacock and Weidman (2005). Because of the presence of the sine and cosine functions, these waves can only exist for certain frequencies ω . Figure 9 shows that two distinct regions of existence in the (ω, Ω) plane are defined by the lines $\omega = \pm N$ and $\omega = 2 \pm \Omega$. In each domain, a typical dispersion relation curve can be plotted. Figure 10 gives some example of these curves in both cases.

5 Waves in Differentially Rotating Flows

Evaluating the dispersion relation of waves when the rotation of the flow is not a solid-body rotation but depends upon the radius: $\Omega = f(r)$ is more tricky. The equation of motion must be written in the stationary frame of reference:

$$\frac{\partial \vec{u}}{\partial t} + (\vec{u} \cdot \vec{\nabla}) \vec{u} + (\vec{u} \cdot \vec{\nabla}) \vec{U} = -\frac{\vec{\nabla} p}{\rho} \quad (19)$$

Fig. 10 Some dispersion relation curves of the gravito-internal waves as functions of axial wavenumber γ for various α and β . In this case, N was chosen equal to $\pm 4 \Omega$ for the curves outside the range $[-2\Omega, 2\Omega]$ (solid curve), and equal to $\pm 0.3 \Omega$ for the curves inside the range $[-2\Omega, 2\Omega]$ (dashed curves)



The difficulty in the calculation of the dispersion relations of these inertial waves comes from the nonlinear advective term that this time, possesses a new term coming from the variation of Ω with r . However, the problem can be solved if we search for solutions in the form of waves, but where the wave vector also rotates around the axis of rotation of the flow:

$$\begin{cases} \frac{\partial \alpha}{\partial t} + \Omega \beta = 0 \\ \frac{\partial \beta}{\partial t} + \Omega \alpha = 0 \\ \frac{\partial \gamma}{\partial t} = 0 \end{cases} \quad (20)$$

Using this property, it can be shown that $\frac{x}{r} = \frac{\alpha}{a}$ and $\frac{y}{r} = \frac{\beta}{a}$, where a is the norm of the projection of the wavevector in the plane perpendicular to the rotation axis: $a^2 = \alpha^2 + \beta^2$. The equations of motion can then be written under the form:

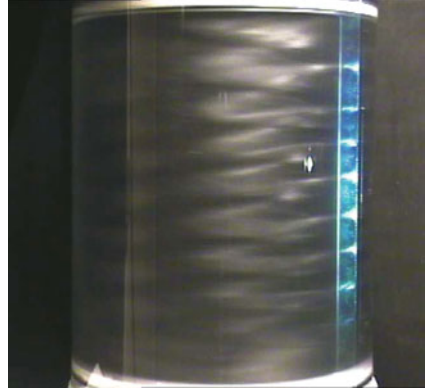
$$\begin{cases} -i\omega \hat{u} & -\Omega \hat{v} + \frac{y}{a} \gamma \frac{d\Omega}{dr} \hat{w} & = -i\alpha \hat{p} \\ -i\omega \hat{v} + \Omega \hat{u} & -\frac{x}{a} \gamma \frac{d\Omega}{dr} \hat{w} & = -i\beta \hat{p} \\ -i\omega \hat{w} & & = -i\gamma \hat{p} \end{cases} \quad (21)$$

Again, using that $\frac{x}{r} = \frac{\alpha}{a}$ and $\frac{y}{r} = \frac{\beta}{a}$, the y and x terms can be transformed. The dispersion relation of inertial waves (at radius r) in a differentially rotating flow can then be calculated after some algebra:

$$\omega^2 = \frac{2\Omega(2\Omega + r \frac{d\Omega}{dr})\gamma^2}{\alpha^2 + \beta^2 + \gamma^2} \quad (22)$$

As can be seen from the above equation, we retrieve the original Kelvin wave dispersion relation when Ω is constant. Also, we can observe that ω is a complex number when $\Omega(2\Omega + r \frac{d\Omega}{dr}) < 0$ which is nothing else than the Rayleigh criterium

Fig. 11 The Strato-Rotational Instability between differentially rotating cylinders (Le Bars and Le Gal 2007)



for the appearance of the centrifugal instability in a rotating flow. Any inviscid flow rotating with a differential rotation $\Omega = f(r)$, is unstable if its angular momentum is a decreasing function of r .

If the flow is furthermore axially stratified, the dispersion relation of these waves can also be calculated. It takes the following form:

$$\omega^2 = 2\Omega \left(2\Omega + r \frac{d\Omega}{dr} \right) \cos^2(\theta) + N^2 \sin^2(\theta) \quad (23)$$

where θ is as before the angle of the wavevector versus the rotation axis of the flow. As can be seen on this equation, the stratification term is positive and thus stabilizes the flow as soon as $\theta \neq 0$. However, if $\theta = 0$, as it is the case for Taylor-Couette vortices, stratification has no effect on the threshold of the centrifugal instability at least at this first order of calculation. A new instability has been however discovered analytically recently (Molemaker et al. 2001). This instability comes from a resonant interaction of the gravito-inertial waves and was named the SRI. It was then studied numerically by Shalybkov and Rüdiger (2005) and experimentally by Le Bars and Le Gal (2007). Figure 11 illustrates the SRI instability in a cylindrical Couette flow. As can be observed, two counter-rotating helices propagate in the gap between both cylinders and produce a braided pattern.

Note that this instability was further studied in the case where the flow is not confined between two walls (Riedinger et al. 2011). This case is particularly interesting for modelling the stability of accretion disks around stars as the laminar Kepler flow of the rotating gas cloud ($\Omega(r) \sim r^{-3/2}$) is stable versus the Rayleigh criterium. Another famous instability which is often invoked for the destabilization of accretion disks, is the so-called Magneto-Rotational Instability MRI (Balbus and Hawley 1998). As we will see in next paragraph, contrary to the SRI, the MRI directly affects the Rayleigh criterium of rotating flows.

6 Alfven and Magneto-Inertial Waves

Now the fluid is considered to be a perfect electric conductor. This framework is called the Ideal Magneto-Hydrodynamics limit. If the viscous effects are still neglected, the linearized Euler equation describes the fluid motions with an additional Lorentz force generated by an imposed axial homogeneous magnetic field \vec{B} . The second equation is the induction equation for the magnetic fluctuations \vec{b} and is reduced in this case to the induction of the magnetic field by the flow perturbations:

$$\begin{cases} \frac{\partial \vec{u}}{\partial t} = -\frac{1}{\rho} \vec{\nabla} p + \frac{\vec{F}}{\rho} \\ \frac{\partial \vec{b}}{\partial t} = (\vec{B} \cdot \vec{\nabla}) \vec{u} \end{cases} \quad (24)$$

with $\vec{F} = \vec{J} \wedge \vec{b}$ where \vec{J} is the electric current density given by $\vec{J} = \frac{\vec{\nabla} \wedge \vec{b}}{\mu}$, where μ is the magnetic diffusivity. Solving these equations with plane waves for \vec{u} and \vec{B} leads to:

$$\begin{cases} -\omega \hat{u} = \frac{B}{\rho \mu} (\gamma \hat{b}_y - \alpha \hat{b}_z) - \alpha \hat{p} \\ -\omega \hat{v} = \frac{B}{\rho \mu} (\gamma \hat{b}_x - \beta \hat{b}_z) - \beta \hat{p} \\ -\omega \hat{w} = -\gamma \hat{p} \end{cases} \quad (25)$$

and

$$\begin{cases} -\omega \hat{b}_x = B \gamma \hat{u} \\ -\omega \hat{b}_y = B \gamma \hat{v} \\ -\omega \hat{b}_z = B \gamma \hat{w} \end{cases} \quad (26)$$

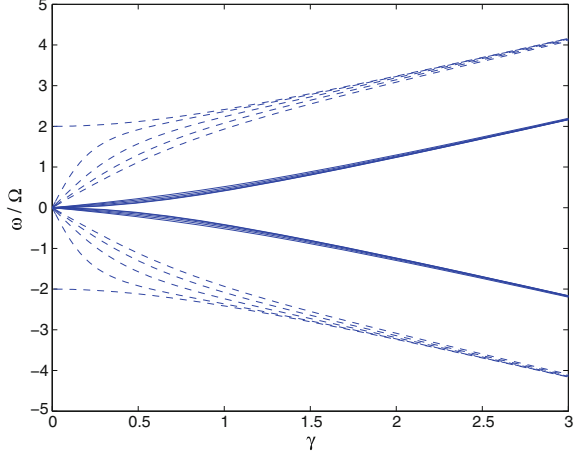
The dispersion relation of Alfven waves with the associated Alfven phase speed V_A is then easily deduced (Alfven 1942):

$$\omega^2 = \frac{B^2}{\rho \mu} \gamma^2 \quad V_A = \frac{B}{\sqrt{\rho \mu}} \quad (27)$$

The linear form of Alfven waves dispersion relation shows that these waves are not dispersive and propagate at a constant Alfven speed V_A . Although these waves are known in astrophysics for a long time (Tsurutani et al. 2005), it is only recently that these waves have been observed in a laboratory experiment (Alboussière et al. 2011). Note that the Alfven speed is around 1 m/s for liquid Gallium under a magnetic field of 0.1 Tesla.

When rotation is added to the flow of conducting fluid, the Coriolis terms need to be incorporated into the equations of motion that become in the Fourier space:

Fig. 12 Some dispersion relation curves of the magneto-internal waves as functions of axial wavenumber γ for various α and β . In this case V_A was chosen equal to $\Omega\gamma$



$$\begin{cases} \omega\hat{u} = 2i\Omega\hat{v} - \frac{B^2\gamma^2}{\rho\mu\omega}\hat{u} + \frac{B^2\gamma\alpha}{\rho\mu\omega}\hat{w} + \alpha\hat{p} \\ \omega\hat{v} = -2i\Omega\hat{u} + \frac{B^2\gamma^2}{\rho\mu\omega}\hat{v} - \frac{B^2\gamma\alpha}{\rho\mu\omega}\hat{w} + \beta\hat{p} \\ \omega\hat{w} = \gamma\hat{p} \end{cases} \quad (28)$$

The analytical formula for the dispersion relation can be calculated and takes the following form:

$$\omega^2 = \frac{\gamma^2}{k^2} \left(V_A^2 k^2 + 2\Omega^2 \pm 2\Omega\sqrt{k^2 V_A^2 + \Omega^2} \right) \quad (29)$$

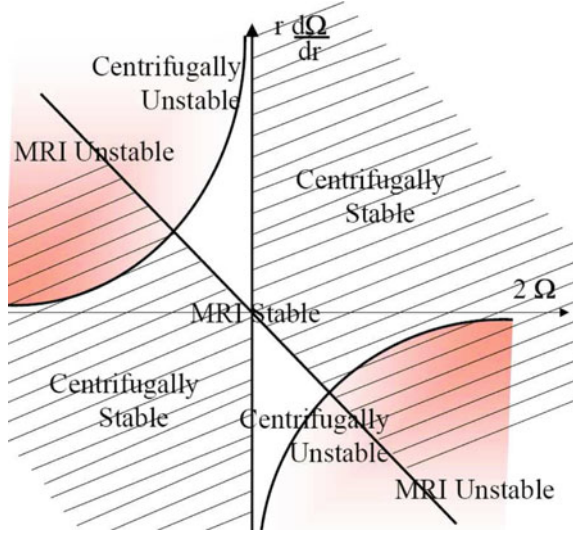
where $k^2 = \alpha^2 + \beta^2 + \gamma^2$ is the square of the norm of the wavenumber and $V_A = \frac{B}{\sqrt{\rho\mu}}$ the Alfvén speed as before. These waves are called Magneto-inertial waves or Magneto-Coriolis waves and their dispersion relation can be plotted the same way it was for pure inertial waves. As observed in Fig. 12, two kinds of branches (the magnetic (solid curves) or the hydrodynamic branches (dashed curves)) can be distinguished. As can be seen by the curvature of the curves, the magneto-inertial waves are dispersive except when the rotation of the flow is dominated by the magnetic field effect where the Alfvén waves characteristics are recovered at large γ .

This dispersion relation formula can then be extended to non solid body rotation cases when introducing the axial vorticity $\Omega_z = \Omega + r\frac{d\Omega}{dr}$, already calculated in Sect. 5. The dispersion relation then becomes:

$$\omega^2 = \frac{\gamma^2}{k^2} \left(V_A^2 k^2 + \Omega\Omega_z \pm \Omega\sqrt{4k^2 V_A^2 + \Omega_z^2} \right) \quad (30)$$

This dispersion relation formula shows in particular that ω^2 can become negative and thus the flow be unstable if $V_A^2 k^2 < -2r\Omega\frac{d\Omega}{dr}$. This criteria replaces the Rayleigh criteria for the centrifugal instability and gives the threshold of the Magneto-Rotational Instability which has a tremendous importance in astrophysics in particular for

Fig. 13 Stability thresholds for the centrifugal (Rayleigh criterium) and the Magneto-Rotational Instability in the $(2\Omega, r \frac{d\Omega}{dr})$ plane. The *straight line* is the Rayleigh criterium and the hyperbolas correspond to the MRI threshold for given magnetic Alfven speed and non zero wave number. We observe that a stable centrifugal inviscid flow can become MRI unstable in the *colored* and *hatched* region in the limit of ideal MHD



the destabilization of accretion disks (Balbus and Hawley 1998). We can plot for a given r both stability thresholds in the plane $(2\Omega, r \frac{d\Omega}{dr})$. Figure 13 shows these limits for given magnetic Alfven speed and non zero wave number. In particular, we can notice that a centrifugally stable flow can indeed be destabilized by the effect of an imposed magnetic field in the colored and hatched zones of the diagram. As can be seen on the figure the smallest Ω is given by the equality of both criteria. Supposing that the smallest wavelength in the device of typical length L is $k = \pi/L$, it is easy to see that the smallest velocity reached in the flow is $V = 2\pi\Omega R = \pi^2 V_A$. As seen before, the order of magnitude of the Alfven speed V_A is 1 m/s in Gallium liquid metal under a magnetic field of 0.1 Tesla. This gives a minimum experimental velocity of 10 m/s and shows the extreme difficulties of designing such a liquid metal experiment. Despite these technical difficulties, several experiments are attempting today to reproduce this instability in Taylor-Couette flow devices, using Sodium as working fluid (Sisan et al. 2004; Stefani et al. 2009).

7 Conclusion

Considering several generic cases of rotating flows, the dispersion relations of different types of waves have been derived from the linearized equations of motion. First inertial or Kelvin waves that propagate in solid body rotating flows were introduced. The 2D version of these waves, known as Rossby waves, that propagate in shallow layers when taking account the so called β effect, was then derived. Pure inertial waves were further enriched by the effect of first a density stratification, then by a non homogeneous rotation and finally by the application of

a magnetic field. The Rayleigh criterium for the inviscid threshold of the centrifugal instability was recovered from these dispersion relations and compared to the Magneto-Rotational Instability threshold. Besides, it was moreover shown that the Strato-Rotational Instability is not caused by a modification of the Rayleigh discriminant inequality but by a resonant phenomenon of gravito-inertial waves that can destabilize a centrifugally stable Taylor-Couette flow.

Especial acknowledgements to Prof. Anne Cros for her kind help during my visit to Mexico. I also thank the Secretaría de Relaciones Exteriores, Dirección General de Cooperación Educativa y Cultural de México for their financial support. I am also grateful to S. Le Dizès for fruitful discussions in the course of preparing this lecture.

References

- Alboussière T, Cardin P, Debray F, La Rizza P, Masson JP, Plunian F, Ribeiro A, Schmitt D (2011) Experimental evidence of Alfvén wave propagation in a Gallium alloy. *Phys Fluids* 23:096601
- Alfvén H (1942) Existence of electromagnetic-hydrodynamic waves. *Nature* 150:405–406
- Balbus SA, Hawley JF (1998) Instability, turbulence, and enhanced transport in accretion disks. *Rev Mod Phys* 70:1–53
- Cébron D, Le Bars M, Leontini J, Maubert P, Le Gal P (2010) A systematic numerical study of the tidal instability in a rotating triaxial ellipsoid. *Phys Earth Planet Inter* 182:119–128
- Courtesy of University of Paris-Sud. <http://www.fast.u-psud.fr/ppcortet/inertialwave.php>
- Courtesy of University of Washington. <http://www.ocean.washington.edu/people/faculty/rhines/rossbypr.html>
- Courtesy of Sakai S, Iizawa I, Aramaki E (1997) Atmosphere and Ocean in a Laboratory: Hokusai. <http://www.gfd-dennou.org/library/gfdexp/expe/exp/iw/1/res.htm>
- Courtesy of University of Oregon (1999). <http://zebu.uoregon.edu/1999/ph161/images/rossbyfor.gif>
- Eloy C, Le Gal P, Le Dizès S (2003) Elliptic and triangular instabilities in rotating cylinders. *J Fluid Mech* 476:357–388
- Kelvin L (1880) Vibrations of a columnar vortex. *Phil Mag* 10:155–68
- Lacaze L, Le Gal P, Le Dizès S (2005) Elliptical instability in a rotating spheroid. *J Fluid Mech* 505:1–22
- Le Bars M, Le Gal P (2007) Experimental analysis of the stratorotational instability in a cylindrical couette flow. *Phys Rev Lett* 99:064502
- Messio L, Morize C, Rabaud M, Moisy F (2008) Experimental observation using particle image velocimetry of inertial waves in a rotating fluid. *Exp Fluids* 44(4):519–528
- Molmaker MJ, McWilliams JC, Yavneh I (2001) Instability and equilibration of centrifugally stable stratified Taylor-Couette flow. *Phys Rev Lett* 86:5270–5273
- Peacock T, Weidman P (2005) The effect of rotation on conical wave beams in a stratified fluid. *Exp Fluids* 39(1):32–37
- Riedinger X, Le Dizès S, Meunier P (2011) Radiative instability of the flow around a rotating cylinder in a stratified fluid. *J Fluid Mech* 672:130–146
- Rossby C-G (1939) Relation between variations in the intensity of the zonal circulation of the atmosphere and the displacements of the semi-permanent centers of action. *J Mar Res* 2(1):38–55
- Shalybkov D, Rüdiger G (2005) Non-axisymmetric instability of density-stratified Taylor-Couette flow. *J Phys* 14:128–137

- Sisan DR, Mujica N, Tillotson WA, Huang YM, Dorland W, Hassam AB, Antonsen TM, Lathrop DP (2004) Experimental observation and characterization of the magnetorotational instability. *Phys Rev Lett* 93:114502
- Stefani F, Gerbeth G, Gundrum T, Hollerbach R, Priede J, Rüdiger G, Szklarski J (2009) Helical magnetorotational instability in a Taylor-Couette flow with strongly reduced Ekman pumping. *Phys Rev E* 80:066303
- Tsurutani BT, Lakhina GS, Pickett JS, Guarnieri FL, Lin N, Goldstein BE (2005) Nonlinear Alfvén waves, discontinuities, proton perpendicular acceleration, and magnetic holes/decreases in interplanetary space and the magnetosphere: intermediate shocks? *Nonlinear Process Geophys* 12:321–326

Fluid Dynamics in Physics, Engineering and
Environmental Applications

Klapp, J.; Medina, A.; Cros, A.; Vargas, C.A. (Eds.)

2013, XXVI, 534 p., Hardcover

ISBN: 978-3-642-27722-1